TECNICA ITALIANA-Italian Journal of Engineering Science
Vol. 61+1, No. 2, December, 2018, pp. 102-114
Journal homepage: http://iieta.org/Journals/TI-IJES

Convective heat transmission inside a porous trapezoidal enclosure occupied by nanofluids: local thermal nonequilibrium conditions for a porous medium

Sheikha M. Al-Weheibi, M. M. Rahman*

Department of Mathematics, College of Science, Sultan Qaboos University, P.O. Box 36, P.C. 123 Al-Khod, Muscat, Sultanate of Oman

Corresponding Author Email: mansur@squ.edu.om

https://doi.org/10.18280/ti-ijes.620208

Received: 10 September 2018
Accepted: 28 October 2018

Keywords:
nanofluid, natural convection, porous medium, right-angle trapezoidal enclosure, thermal nonequilibrium state

ABSTRACT

This study investigates numerically the local thermal nonequilibrium conditions among the Cu-H_2O nanofluid and the Aluminum foam porous matrix for the unsteady free convective flow within an enclosure of right-angle trapezoidal type. For mathematical formulation, the horizontal walls of the enclosure are well-thought-out to be adiabatic while having dissimilar temperatures for the vertical and inclined walls. To gain the physical insight of the problem, the dimensionless constitutive equations are simulated by means of finite element method (FEM) using Comsol Multiphysics a pde solver. For jurisdiction of the obtained numerical results, we compared them with the available works in the literature and a noble covenant is accomplished. The simulated data for isotherms and dimensionless temperature profiles along lines $Y = X$ and $Y = 2X - 0.05$ inside the cavity are displayed for different key parameters. The results show that Nield and Darcy numbers are the key parameters which strongly control the state of local thermal nonequilibrium among the solid matrix and the nanofluid.

1. INTRODUCTION

Nanofluids are new type of fluids [1] engineered by mixing base fluids and solid nanoparticles which exhibit practical uses in innumerable areas of engineering, science and technology [2-3]. Due to the real world applications significant researches have been done on heat transfer in nanofluid in various geometries considering numerous flow and different thermal conditions [4-13]. For the past several years' studies of nanofluids in porous medium became a topic of active research for the scientists and engineers' since their many applications in different fields, such as manufacture of thermal isolators, geothermal systems, drying technologies, cooling of electronic equipment, heat exchangers, nuclear reactors design, solar collectors, etc [14-15]. Vafai [16-17], and Vadasz [18] have documented extensive literature on transport in porous media. Thus, using porous media together with nanofluid is extremely suited for the usage in practical heat transfer procedures due to its large potential for heat transfer augmentation [19-21]. This also obtains a chance for engineers to improve different compact and operative heat transfer devices. It was concluded by many researchers through their potential explorative works that by means of both nanofluids together with porous media enhances the degree of heat transmission in a thermal system [22].

Over the years numerous studies dealing with mechanisms of natural convection heat transfers within a porous media have been conveyed [23-28]. On the other hand; many of these studies considered that saturated fluid and porous matrix are locally in the state of thermal equilibrium (LTE) when studying transport phenomenon in porous media. Studying of convective flow in porous cavities considering the LTE model was the subject through the last periods and that can be found in different review papers like Nield and Bejan [29], and Nield [30]. In fact, in many applications supposition of LTE among the phases of fluid and solid is inappropriate; since the temperatures of nanofluid and porous matrix are unalike, and that causes the local thermally non-equilibrium (LTNE) state. In some practical applications: cooling electronic devices, solar collectors for renewable energy, and cooling of nuclear reactors LTNE model is imperative. Likewise, assumptions of LTNE and LTE amidst the phases of solid and fluid are not sufficient for several applications.

Recently, a number of published papers studying natural convection heat transfer considering the LTNE model are also approved. In this light Al-Amiri [19] used two-energy equations model for the numerical simulation of natural convection heat transfer in a heated square cavity drenched in a permeable medium. An investigation on steady natural convection flow and heat transfer in a square porous enclosure was initiated and explored by Baytas and Pop [31] considering LTNE model to advance the heat transmission rate. They found that consideration of LTNE model amends expressively the flow behavior, especially the local Nusselt number. Hossain and Wilson [32] studied unsteady laminar natural convection flow in a cavity of rectangular type embedded in a fluid-saturated permeable medium considering LTNE model. They presented the effects of internal heat generation and porosity of the medium on both streamlines and isotherms. They compared their results with the results obtained by using the LTE model. Wu et al. [33] have taken into account the LTNE and Brinkman–Forchheimer extended Darcy model and have studied numerically the free convection in a porous rectangular cavity. Using sinusoidal thermal boundary conditions on the vertical walls, they concluded that an increased Nield number as well as thermal conductivity ratio boosted the heat transfer rate. The effect of LTNE state between solid matrix and the saturated fluid in a slender enclosure was investigated numerically by Pippal and Bera [34]. It was reported that heat transmission rate become maximum for the lowest assessment of the aspect ratio irrespective of the types of states whether LTE or LTNE. Mahmoudi et al. [35] studied heat transfer in a channel partially filled with porous medium considering LTNE model. It was established that rate of heat transfer highly affected by the applied interface model. Sheremet et al. [36] used the Tiwari and Das [37] nanofluid model and studied convective heat transfer in a square porous enclosure considering two temperature equations: one for nanofluid and other for the solid matrix. They found that increased nanoparticles volume fraction represses the convective flow. On the other hand Nield number decreases the heat transfer rate with the increase of it. Recently, Sheikholeslami and Shehzad [38] have used two-temperature model and investigated convective heat transfer flow of nanofluid in a porous enclosure. They obtained an opposite relationship between the temperature gradient and the porosity. Mehryan et al. [39] studied convective flow of micropolar nanofluid in a porous enclosure considering LTNE model. They reported that nanofluid flow can be modeled through the classical Navier-Stokes equations when the porosity of the medium is large.

From the above-literature review, we notice that the conditions for the existence of LTNE and LTE among the solid matrix and the nanofluid are not yet reported. It is very important to detremine the conditions and identify the key model parameters which will regulate the heat exchange between the nanofluid and the solid matrix to reach in LTNE or LTE states when modeling nanofluid flow in a porous medium. This is the main focus of this research. Thus, a numerical study is piloted using Darcy-Brinkman model to investigate the convective flow and heat transfer mechanisms in a nanofluid saturated porous right-angle trapezoidal cavity considering LTNE among the porous matrix and passing nanofluid taking into account Tiwari and Das [37] model.

2. PHYSICAL MODEL

2.1 Model specification

We study convective flow in a right-angle trapezoidal enclosure implanted in a homogeneous porous medium occupied by incompressible nanofluids. The flow inside the enclosure is anticipated to be two-dimensional, unsteady, and laminar. The Cartesian coordinates: x-axis is assumed along the bottom horizontal wall of the enclosure while the y-axis is perpendicular to it. The gravity is acted along the negative y-axis. The lengths of the right vertical, bottom and upper walls are H, L and l, respectively, where $L > l$. The top and bottom walls of the cavity are thermally insulated; while the left inclined and right vertical side walls of the cavity are kept at uniform temperatures T_h and T_c, respectively. In all circumstances, $T_h > T_c$ is upheld. All boundaries of the trapezoidal enclosure are supposed to be rigid and there are no-slips on them. The diagram of the model along with coordinates system is shown in Figure 1. We considered that nanoparticles and base fluids are in thermal equilibrium and there is no-slip among them. We further considered that temperatures of the porous matrix and passing nanofluid are dissimilar i.e. they are in local thermal nonequilibrium state and the pores are uniform. For numerical simulation Cu-H_2O nanofluid is used with Aluminum foam as a porous medium.

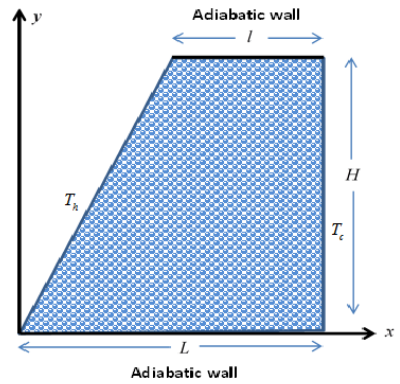

Figure 1. Schematic view of the physical model

2.2. Mathematical modeling

Following afore-said assumptions and taking into account the Darcy-Brinkman model for transport in porous media [40-41]; the dimensional equations which govern the present study are as follows [36−37]:

$$\frac{\partial u}{\partial x}+\frac{\partial v}{\partial y}=0 \tag{1}$$

$$0=-\frac{\partial p}{\partial x}-\frac{\mu_{nf}}{K}u+\tilde{\mu}_{nf}\left(\frac{\partial^2 u}{\partial x^2}+\frac{\partial^2 u}{\partial y^2}\right) \tag{2}$$

$$0=-\frac{\partial p}{\partial y}-\frac{\mu_{nf}}{K}v+\tilde{\mu}_{nf}\left(\frac{\partial^2 v}{\partial x^2}+\frac{\partial^2 v}{\partial y^2}\right)+(\rho\beta)_{nf}\,g(T_{nf}-T_0) \tag{3}$$

$$\frac{\partial T_{nf}}{\partial t}+\frac{1}{\varepsilon}\left(u\frac{\partial T_{nf}}{\partial x}+v\frac{\partial T_{nf}}{\partial y}\right)=\frac{k_{nf}}{(\rho C_p)_{nf}}\left(\frac{\partial^2 T_{nf}}{\partial x^2}+\frac{\partial^2 T_{nf}}{\partial y^2}\right)+\frac{h}{\varepsilon(\rho C_p)_{nf}}(T_s-T_{nf}) \tag{4}$$

$$\frac{\partial T_s}{\partial t}=\frac{k_s}{(\rho C_p)_s}\left(\frac{\partial^2 T_s}{\partial x^2}+\frac{\partial^2 T_s}{\partial y^2}\right)+\frac{h}{(1-\varepsilon)(\rho C_p)_{nf}}(T_{nf}-T_s) \tag{5}$$

Here u and v are the velocity components along the x - and y - axes respectively, g is the acceleration due to gravity, p is the pressure, T_{nf} is the temperature of the nanofluid, T_s is the temperature of the solid matrix, $T_0=\frac{T_h+T_c}{2}$ is the reference temperature where T_h is the temperature of the hot wall and T_c is the temperature of the cold wall, ρ_{nf} is the density of nanofluid, $(\rho C_p)_{nf}$ is the heat capacity of nanofluid, $(\rho C_p)_s$ is the heat capacity of solid matrix, t is the time, k_{nf} is the thermal conductivity of nanofluid, k_s is the thermal conductivity of the solid matrix, h is the interface heat transfer coefficient between the nanofluid and solid matrix, ε is the porosity, μ_{nf} is the dynamic viscosity of nanofluid, and $\tilde{\mu}_{nf} = \mu_{nf}/\varepsilon$ is the effective viscosity [42] in a porous medium.

2.3 Thermophysical properties of nanofluids

The thermal performance of a nanofluid depends on its thermophysical properties such as density, viscosity, thermal conductivity, heat capacitance, thermal diffusivity, and thermal expansion coefficient. In the present study the following correlations are used for them:

$$\rho_{nf} = (1-\phi)\rho_{bf} + \phi\rho_{sp} \quad [37] \tag{6}$$

$$\frac{\mu_{nf}}{\mu_{bf}} = \frac{1}{(1-\phi)^{2.5}} \quad [43] \tag{7}$$

$$\frac{k_{nf}}{k_{bf}} = \frac{k_{sp} + 2k_{bf} - 2(k_{bf} - k_{sp})\phi}{k_{sp} + 2k_{bf} + (k_{bf} - k_{sp})\phi} \quad [44] \tag{8}$$

$$(\rho Cp)_{nf} = (1-\phi)(\rho Cp)_{bf} + \phi(\rho Cp)_{sp} \quad [14] \tag{9}$$

$$\alpha_{nf} = \frac{k_{nf}}{(\rho Cp)_{nf}} \quad [37] \tag{10}$$

$$(\rho\beta)_{nf} = (1-\phi)(\rho\beta)_{bf} + \phi(\rho\beta)_{sp} \tag{11}$$

Here ϕ is the nanoparticles volume fraction. The definitions of the variables and their units are are listed in the nomenclature. In Table 1 we have listed the effective thermophysical properties of Cu-H_2O nanofluid [45] and Aluminum foam (AF).

Table 1. Thermophysical properties of Cu-H_2O nanofluid and Aluminum foam (AF)

Thermo-physical properties	H_2O	Cu	AF
C_p	4179	385	897
ρ	997.1	8933	2700
k	0.613	401	205
μ	0.001003	-	-
$\beta \times 10^{-5}$	21	1.67	-
$\alpha \times 10^{-7}$	1.47	1163.1	-

2.4 Initial and boundary conditions

For

$$t \le 0,\ u = v = p = T_{nf} = T_s = 0 \tag{12}$$

The boundary conditions as shown in Figure 1 for $t > 0$ are: At the bottom horizontal wall of the cavity: $0 \le x \le L, y = 0$:

$$u = v = 0,\ \frac{\partial T_{nf}}{\partial y} = \frac{\partial T_s}{\partial y} = 0 \tag{13}$$

At the top horizontal wall of the cavity: $L - l \le x \le L, y = H$:

$$u = v = 0,\ \frac{\partial T_{nf}}{\partial y} = \frac{\partial T_s}{\partial y} = 0 \tag{14}$$

At the left inclined wall of the cavity: $0 \le x \le L - l, y = \frac{H}{L-l}x$:

$$u = v = 0,\ T_{nf} = T_s = T_h \tag{15}$$

At the right vertical wall of the cavity: $0 \le y \le H, x = L,$:

$$u = v = 0,\ T_{nf} = T_s = T_c \tag{16}$$

2.5 Dimensionless governing equations

Dimensional analysis gives freedom to analyze a system irrespective of their material properties that constitute it. Dimensionless equations provide an insight of the key controlling parameters of a physical system. The obtained results from these equations do not depend on the size of the physical domain. One can simply get acumen of the physical problem before doing any experiment. Because of these benefits it became an essential mathematical tool for fluid mechanics.

To make the governing equations dimensionless we introduce the following:

$$\left.\begin{aligned} & X = \frac{x}{L}, Y = \frac{y}{L}, U = \frac{u}{(\alpha_{bf}/L)}, V = \frac{v}{(\alpha_{bf}/L)}, \\ & \tau = \frac{t\alpha_{bf}}{L^2}, P = \frac{pK}{\mu_{bf}\alpha_{bf}}, \theta_{nf} = \frac{T_{nf} - T_0}{T_h - T_c}, \\ & \theta_s = \frac{T_s - T_0}{T_h - T_c}, T_0 = \frac{T_h + T_c}{2} \end{aligned}\right\} \tag{17}$$

Using (17) into (1)-(5), we obtain the nondimensional governing equations as follows:

$$\frac{\partial U}{\partial X} + \frac{\partial V}{\partial Y} = 0 \tag{18}$$

$$0 = -\frac{\partial P}{\partial X} - \frac{\mu_{nf}}{\mu_{bf}}U + \left(\frac{Da}{\varepsilon}\frac{\mu_{nf}}{\mu_{bf}}\right)\left(\frac{\partial^2 U}{\partial X^2} + \frac{\partial^2 U}{\partial Y^2}\right) \tag{19}$$

$$\begin{aligned} 0 = -\frac{\partial P}{\partial Y} - \frac{\mu_{nf}}{\mu_{bf}}V + \left(\frac{Da}{\varepsilon}\frac{\mu_{nf}}{\mu_{bf}}\right)\left(\frac{\partial^2 V}{\partial X^2} + \frac{\partial^2 V}{\partial Y^2}\right) \\ + \frac{(\rho\beta)_{nf}}{(\rho\beta)_{bf}} Da\,\mathrm{Ra}\,\theta \end{aligned} \tag{20}$$

$$\begin{aligned} & \varepsilon\frac{\partial \theta_{nf}}{\partial \tau} + U\frac{\partial \theta_{nf}}{\partial X} + V\frac{\partial \theta_{nf}}{\partial Y} \\ & = \varepsilon\left(\frac{\alpha_{nf}}{\alpha_{bf}}\right)\left(\frac{\partial^2 \theta_{nf}}{\partial X^2} + \frac{\partial^2 \theta_{nf}}{\partial Y^2}\right) + Ni\frac{(\rho Cp)_{bf}}{(\rho Cp)_{nf}}(\theta_s - \theta_{nf}) \end{aligned} \tag{21}$$

$$\lambda\frac{\partial \theta_s}{\partial \tau} = \left(\frac{\partial^2 \theta_s}{\partial X^2} + \frac{\partial^2 \theta_s}{\partial Y^2}\right) + \frac{1}{(1-\varepsilon)} Ni\ \delta(\theta_s - \theta_{nf}) \tag{22}$$

where $D_a = \frac{K}{L^2}$ is the Darcy number, $R_a = \frac{g\beta_{bf}(T_h - T_c)L^3}{v_{bf}a_{vf}}$ is the Rayleigh number, $N_i = \frac{hL^2}{K_{bf}}$ is the Nield number, $\lambda = \frac{a_{bf}}{a_s}$ is the ratio of diffusivities, and $\delta = \frac{k_{bf}}{k_s}$ is the ratio of conductivities.

Using (17) into (13)-(16), we obtain the following dimensionless boundary conditions

At the bottom wall of the cavity: $0 \le x \le 1, y = 0$

$$U = V = 0,\ \frac{\partial \theta_{nf}}{\partial Y} = \frac{\partial \theta_s}{\partial Y} = 0 \tag{23}$$

At the top wall of the cavity:

$$1 - A_1 \le X \le 1,\ Y = A_2:$$

$$U = V = 0,\ \frac{\partial \theta_{nf}}{\partial Y} = \frac{\partial \theta_s}{\partial Y} = 0 \tag{24}$$

At the left wall of the cavity:

$$0 \le X \le 1 - A_1,\ Y = \frac{A_2}{1 - A_1} X:$$

$$U = V = 0,\ \theta_{nf} = \theta_s = 0.5 \tag{25}$$

At the right wall of the cavity:

$$X = 1,\ 0 \le Y \le A_2:$$

$$U = V = 0,\ \theta_{nf} = \theta_s = -0.5 \tag{26}$$

where $A_1 = \frac{l}{L}$, $A_2 = \frac{H}{L}$, are aspect ratios.

The average Nusselt number is a key parameter that measures the rate of heat transfer from the cavity wall to the fluid as well as to the solid matrix. For nanofluid and solid matrix these numbers are calculated as below

$$Nu_{nf} = -\frac{\kappa_{nf}}{\kappa_{bf}} \int_0^1 \left(\frac{\partial \theta_{nf}}{\partial X} \right) \Bigg|_{Y=(1/(1-A_1))X} dY \tag{27}$$

$$Nu_s = -\int_0^1 \left(\frac{\partial \theta_s}{\partial X} \right) \Bigg|_{Y=(1/(1-A_1))X} dY \tag{28}$$

3. NUMERICAL METHOD

The dimensionless system of governing equations (18)–(22) and boundary conditions (23)–(26) are treated numerically by means of the pde solver "Comsol Multiphysics" that uses FEM of Galerkin type. Zienkiewicz and Taylor [46], Uddin and Rahman [47] and Al-Kalbani et al. [48] gave a well description for the details of this method. For using Comsol Multiphysics it is important to generate mesh, choose suitable solver and then for the convergence of the obtained solution test the grid sensitivity. Moreover, it is good to validate the simulated results with the available numerical data published earlier.

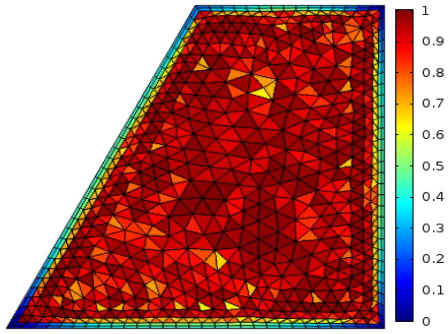

Figure 2(a). Mesh within the cavity

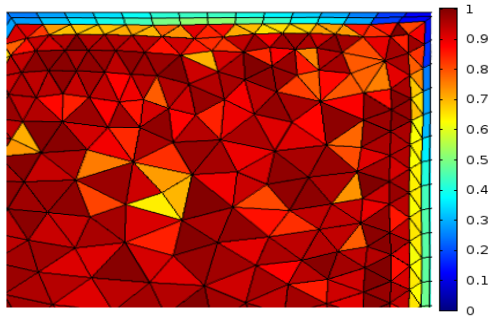

Figure 2(b). Zoom-in the upper right-corner of the cavity

3.1 Construction of meshes

Mesh generation is an important step in FEM that divides the physical domain into a set of sub-domains. The discrete locations in FEM are defined by the numerical grid, at which the variables are to be calculated. Meshing complicated geometry makes FEM a powerful method to handle the boundary value problems in science, engineering and other applications. Figure 2 depicts the grid generation and a legend of quality measure of the cavity.

3.2 Tests for grid sensitivity

A grid independent test is done when $Ra=10^5$, $\emptyset=0.05$, $\varepsilon=0.9$, $Ni=10$, $Da=0.1$, and $\tau=1$. considering Cu-H_2O nanofluid and Aluminum foam as a porous medium inside the cavity. Five non-uniform grids such as normal, fine, finer, extra fine and extremely fine were tested having 1241, 1988, 5547, 14610, and 20954, respectively, number of elements within the resolution field.

Table 2. Grid sensitivity test for Cu-H_2O nanofluid and Aluminum foam at $Ra=10^5$, $\emptyset=0.05$, $\varepsilon=0.9$, $Ni=10$, $Da=0.1$, and $\tau=1$

Number of elements	1241	1988	5547	14610	20954
Nu_{nf}	3.68865	4.26618	4.47556	4.47603	4.47649
Nu_s	1.31327	1.31405	1.31643	1.31764	1.31764

The numerical experiment is done calculating the average Nusselt number displayed in Table 2 on the left inclined wall of the cavity for the aforementioned elements to test the grid fineness. The average Nusselt numbers for 14610 elements show a high accuracy when compared with the corresponding results of 20954 elements. Therefore, either of 14610 and 20954 grid elements guarantees the results with certain accuracy. In our study we used 14610 elements for the numerical simulation.

3.3 Corroboration of the numerical code

Due to the scarcity of the experimental data, the current simulated results were compared with the numerical results of Sheremet et al. [36] for a special case. They studied steady free convection flow in a square enclosure filled with Cu-H_2O nanofluid and aluminum foam as solid matrix when the model parameters are $Ra=10^3$, $\emptyset=0.05$, $\varepsilon=0.9$ and $Ni=100$. The comparison among the data presented in Table 3 gives a good agreement with our study. This corroboration lifts the assurance in using the current code.

Table 3. Average Nusselt numbers Nu_{nf} and Nu_s of Sheremet et al. [36] (1st row) in comparison with the present results (2nd row) when $Ra=10^3$, $\emptyset=0.05$, $\varepsilon=0.9$, and $Ni=100$

Authors	Nu_{nf}	Nu_s
Sheremet et al. [36]	8.296	1.1324
Present results	8.39599	1.13427

4. RESULTS AND DISCUSSION

In this section we analyzed the simulated results to investigate the local thermal nonequilibrium (LTNE) conditions for a free convective heat transfer flow of nanofluid inside the right-angle trapezoidal enclosure in a porous medium. The default parameter values for the numerical simulations are considered to be $Ra=10^5$, $Da=0.1$, $Ni=10$, $\varepsilon=0.6$, $\emptyset=0.05$, and $\tau=1$ (steady state) unless otherwise specified and all calculation are taken considering Cu-H_2O nanofluid with Aluminum foam as a porous medium. The effects of the key parameters such as Nield number, Darcy number, porosity of the porous medium and the nanoparticles volume fraction on the temperature distributions of the nanofluid in addition to the solid matrix along the lines *Y=X* and *Y=2X-0.05* are presented graphically with the parameter range $(10 \leq Ni \leq 10^5)$, $(10^{-5} \leq Da \leq 10^{-1})$, $0.4 \leq \varepsilon \leq 0.9$, and $0 \leq \emptyset \leq 0.1$.

Figures 3(a)-(d) and 4(a)-(d) display the variations of isotherms of both nanofluids, and porous matrix within the cavity varying Nield number. It is found that isotherms of nanofluid typify a reduction in the heat transfer rate by aggregating the Nield number. It is also found that isotherms in fluid phase reveal a convective heat transfer that is week whereas in the solid phase it is intensive. That is due to the intensification in the heat transfer rate among the nanofluid and the porous matrix.

For large Nield number ($Ni = 10^5$) it is obvious that the isotherms of nanofluid and solid matrix are alike. In other words, the temperature distributions in the enclosure are analogous which denotes obviously that the nanofluid and solid matrix are reached to the LTE state which can be investigated clearly from Figures 5(a)-(c) and 6(a)-(c). In Figures 5(a)-(c) and 6(a)-(c), the dimensionless temperature profiles varying Nield number along the diagonal (Y=X) of the cavity as well as along the line (Y=2X-0.05) which is close to the heated wall of the enclosure are plotted for both nanofluid and solid matrix. We found that when Da is large (Da=0.1) for small values of *Ni* the nanofluid and the solid matrix are in LTNE. It can be observed that both temperature profiles (θ_{nf}, θ_s) coincide with each other for larger values of the Nield number ($Ni \geq 10^5$) along the two lines which is a clear indication that the nanofluid and the solid matrix are at LTE state.

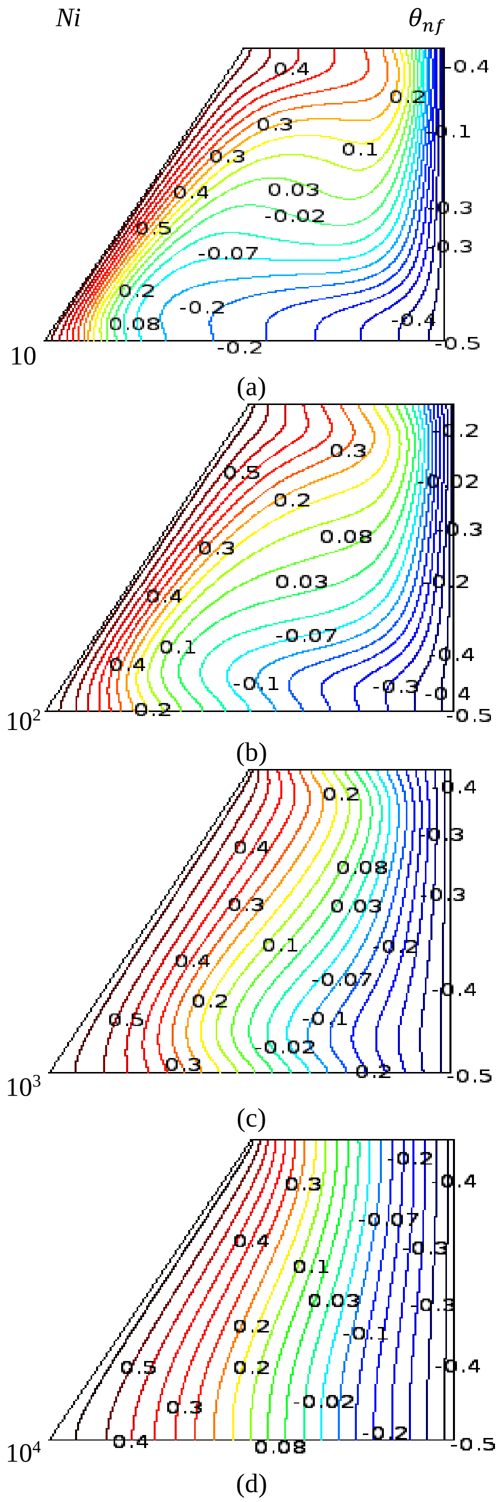

Figures 3(a)-(d). Isotherms of nanofluid for different values of the Nield number when $Ra=10^5$, $\emptyset=0.05$, $\varepsilon = 0.6$, $Da=0.1$ and $\tau=1$

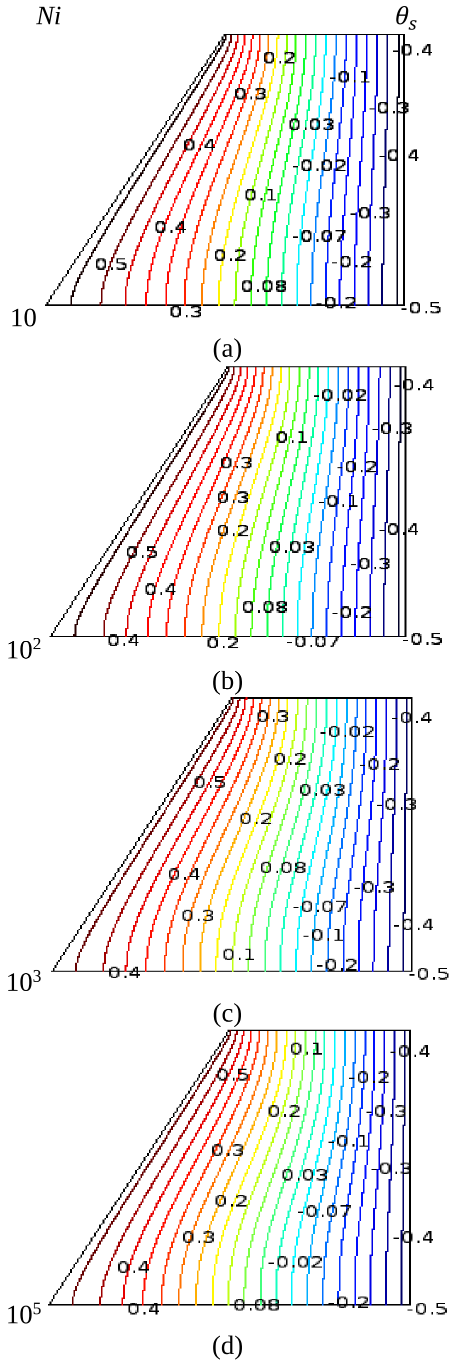

Figures 4(a)-(d). Isotherms of porous matrix for different values of the Nield number when Ra=10^5, ∅=0.05, $\varepsilon = 0.6$, Da=0.1 and τ=1

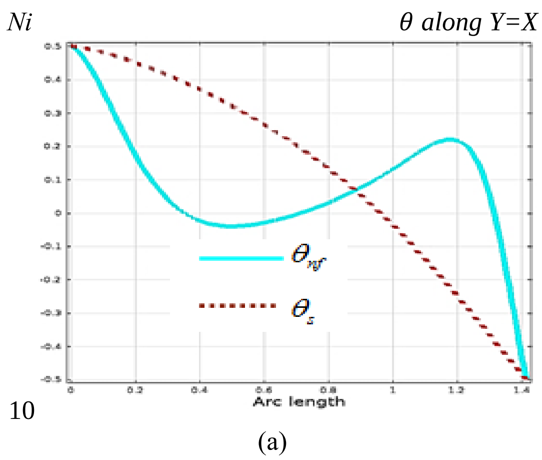

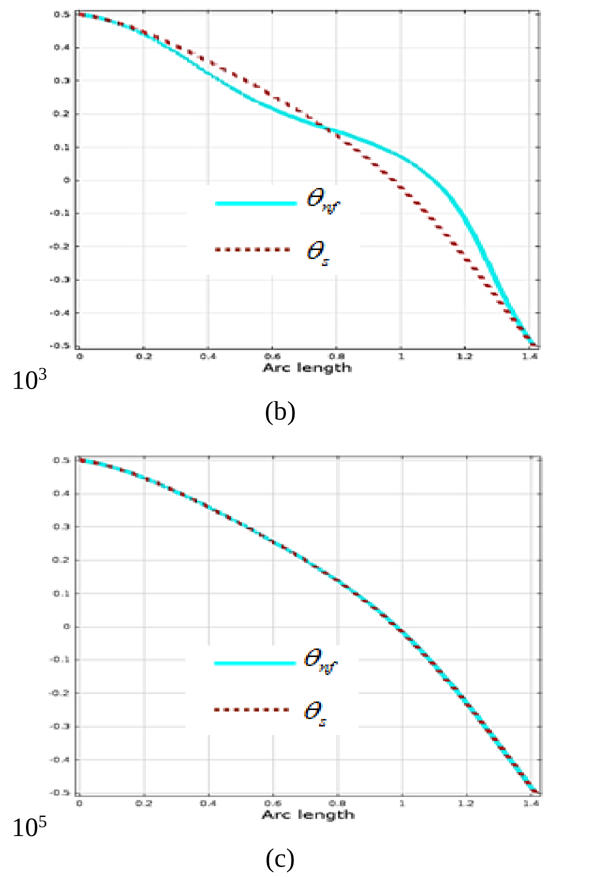

Figure 5(a)-(c). Temperature distributions along the lineY=X as a function of arc length varying Nield number when Ra=10^5, ∅=0.05, $\varepsilon = 0.6$, Da=0.1 and τ=1

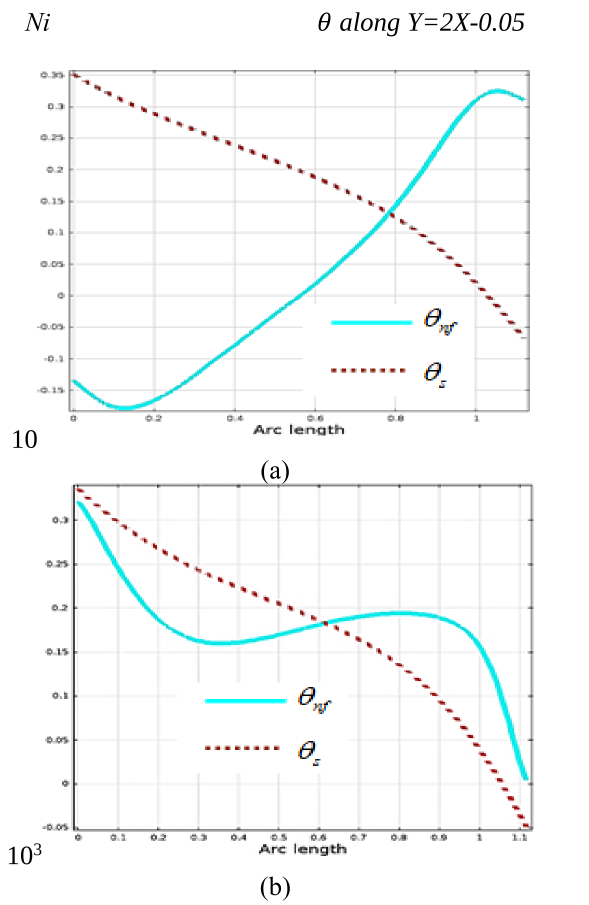

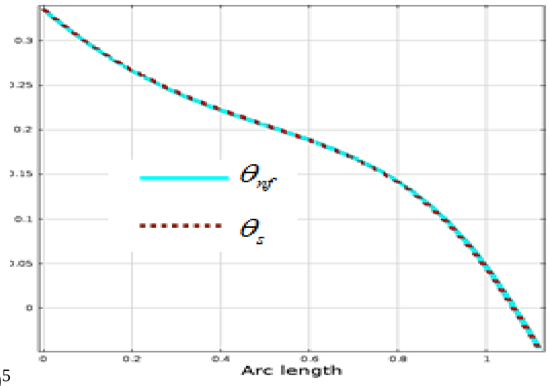

10^5

(c)

Figure 6(a)-(c). Temperature distributions along the lineY=2X-0.05 as a function of arc length varying Nield number when Ra=10^5, ∅=0.05, $\varepsilon = 0.6$, Da=0.1 and τ=1

Da *θ along Y=X*

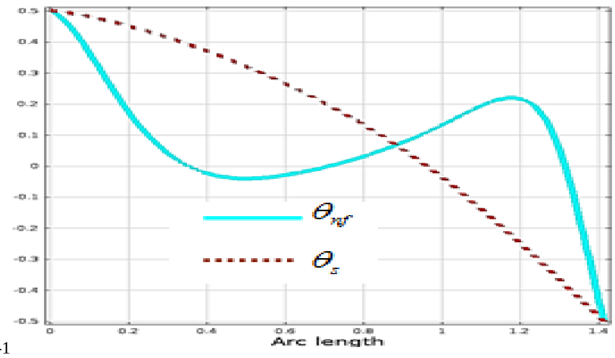

10^{-1}

(a)

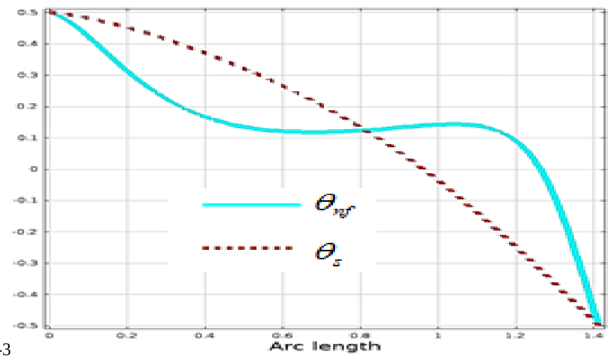

10^{-3}

(b)

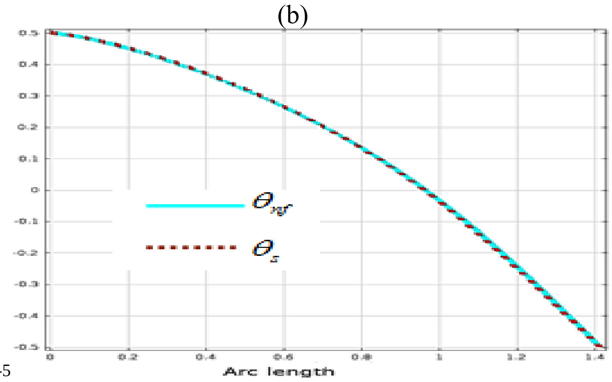

10^{-5}

(c)

Figures 7(a)-(c). Temperature distributions along the line Y=X as a function of arc length varying Darcy number when Ra=10^5, ∅=0.05, $\varepsilon = 0.6$, Ni=10 and τ=1

Da *θ along Y=2X-0.05*

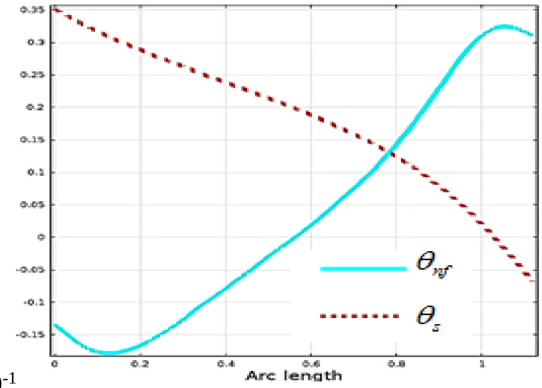

10^{-1}

(a)

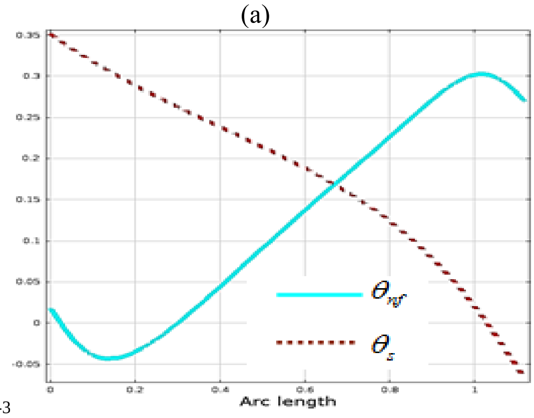

10^{-3}

(b)

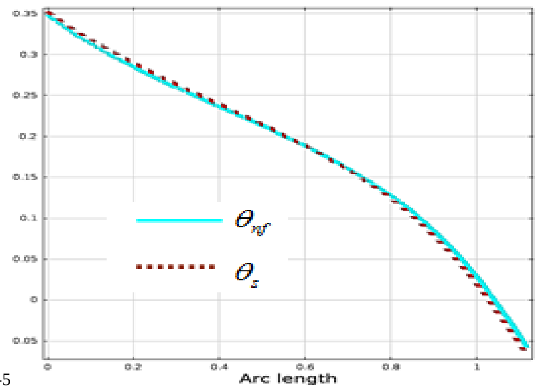

10^{-5}

(c)

Figures 8(a)-(c). Temperature distributions along the line $Y = 2X - 0.05$ as a function of arc length varying Darcy number when Ra=10^5, ∅=0.05, $\varepsilon = 0.6$,Ni=10 and τ=1

Increasing the porousness of a medium i.e. for higher Darcy number (Da $\geq 10^{-5}$) and for smaller Nield number (Ni $= 10$) as in Figures 7(a)-(c) and 8(a)-(c) we can notice that the nanofluid and the solid matrix are in LTNE state. On the other hand, for Darcy number Da $< 10^{-5}$one can observe that both temperature profiles (θ_{nf}, θ_s) match with each other along the two lines which is due to the fact that both nanofluid and the solid matrix are reached at the LTE state. As evidenced from Figures 5 & 6 and 7 & 8 we conclude that the LTE among the nanofluid and the porous matrix highly depends on both the Nield number and the Darcy number. Figures 9(a)-(c) to 12(a)-(c) also confirm the same. When Da $= 10^{-5}$Figures 9(a)-(c) and 10(a)-(c) illustrates that the dimensionless temperature profiles along the diagonal (*Y=X)* and along the line (*Y=2X-*

0.05) are coincide with each other for any values of the Nield number, $(10 \le \mathrm{Ni} \le 10^5)$.

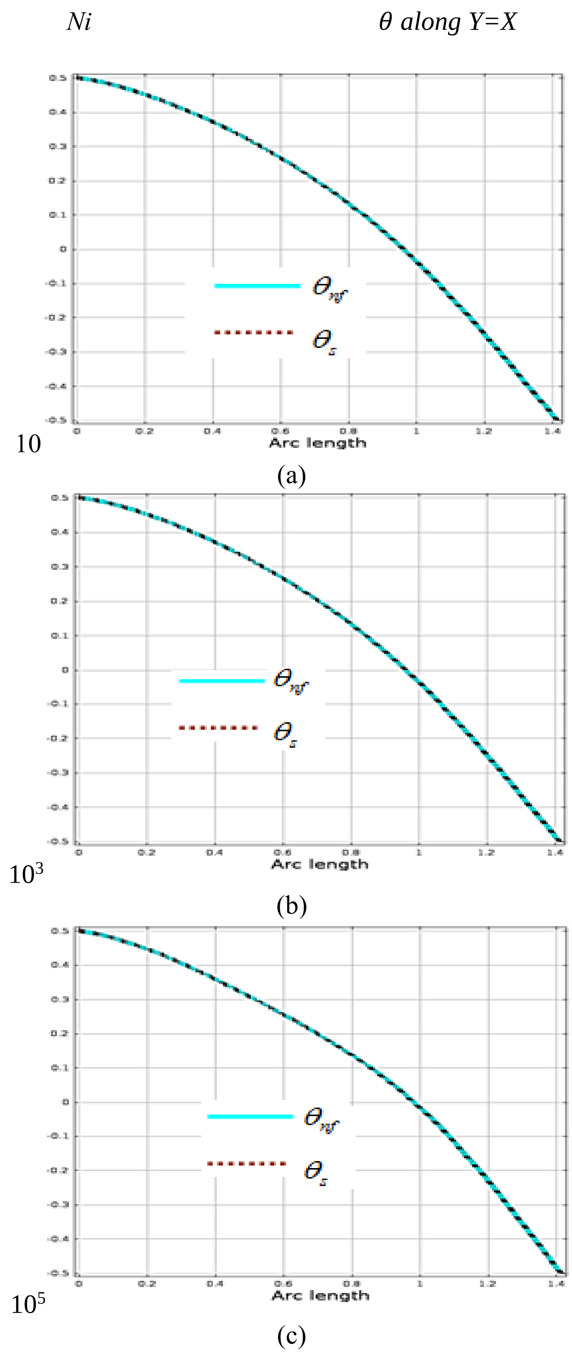

Figures 9(a)-(c). Temperature distributions along the line $Y = X$ as a function of arc length varying Nield number when ∅=0.05, Ra=10^5, τ=1, $\mathrm{Da} = 10^{-5}$, $\varepsilon = 0.6$

Likewise, Figures 11(a)-(c) and 12(a)-(c) show that when $\mathrm{Ni} = 10^5$ and for various values of the Darcy number, $10^{-5} \le \mathrm{Da} \le 10^{-1}$ along the aforesaid two lines both nanofluid and the solid matrix are in the LTE state. Thus, from Figures 3 to 12 and based on the results studied, the domain of LTE and LTNE be influenced by both Nield number and Darcy number. This result is a new finding and has not been reported in the literature before.

Figures 13(a)-(c) demonstrate the influence of nanoparticles volume fraction (∅) on the distributions of temperature of nanofluid and porous matrix along the line (*Y*=*X*). It is clear from this figure that the local thermal exchange between the nanofluid and the porous matrix due to effects of nanoparticles volume fraction (∅) is negligible which can also be clearer from Figures 14(a)-(b) and 15(a)-(b) that show the dimensionless temperature profiles along the diagonal (*Y*=*X*) at the LTNE and LTE domains, respectively. The graphs in the two figures show that the dimensionless temperature profiles for different nanoparticles loading (∅=0,0.025,0.05 and 0.1) coincide with each other for both nanofluid and the porous matrix at LTNE and LTE domains.

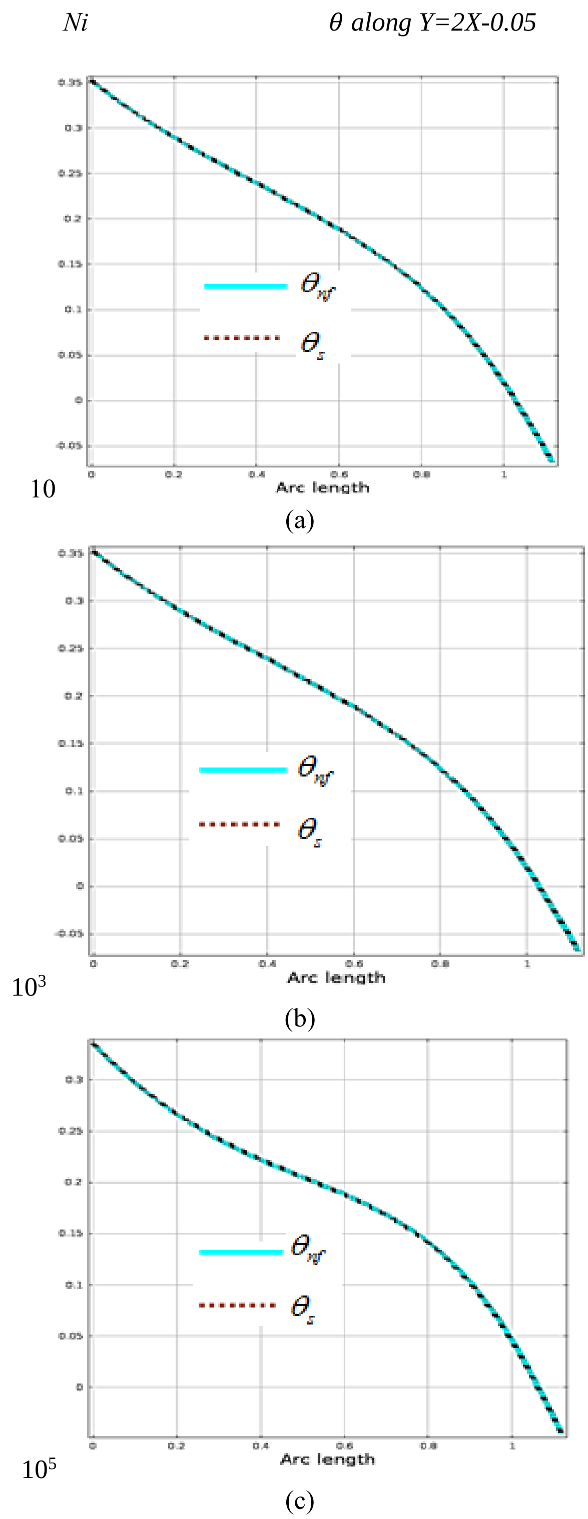

Figures 10(a)-(c). Temperature distributions along the line $Y = 2X - 0.05$ as a function of arc length varying Nield number when Ra=10^5 τ=1 and $\mathrm{Da} = 10^{-5}$, $\varepsilon = 0.6$, ∅=0.05

Da *θ along Y=X*

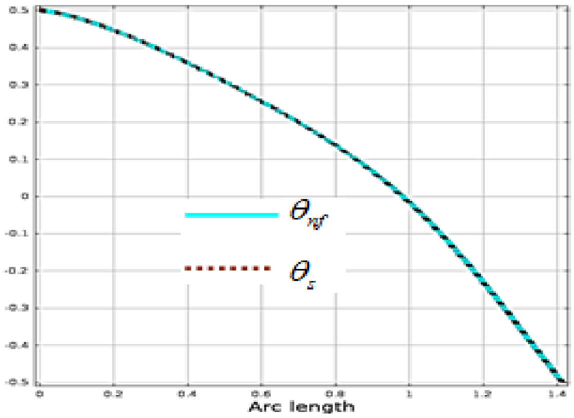

10^{-1}

(a)

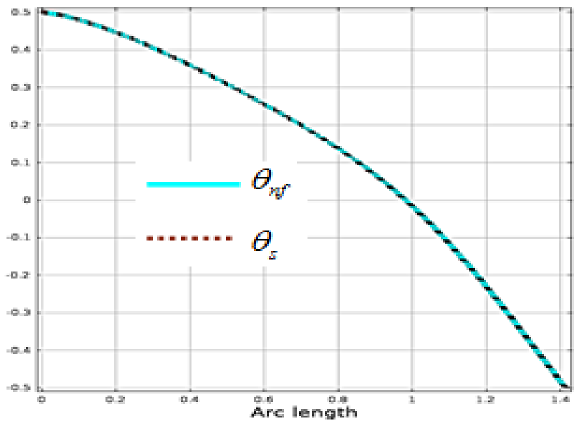

10^{-3}

(b)

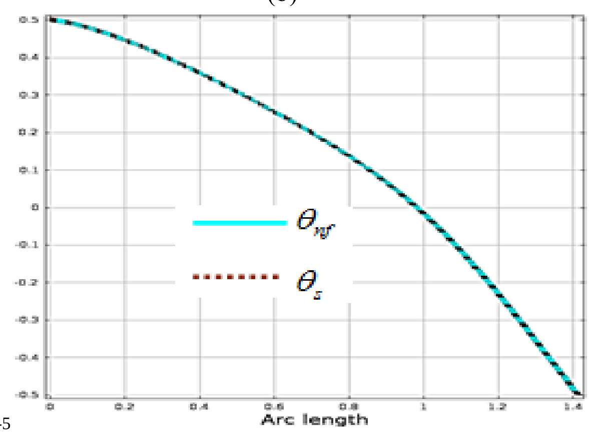

10^{-5}

(c)

Figures 11(a)-(c). Temperature distributions along the line $Y = X$ as a function of arc length varying Darcy number when Ra=10^5 τ=1 and Ni $= 10^5$, ε = 0.6 , Ø=0.05

Similarly, investigating the influence of the porosity (ε) of the porous medium on the temperature distributions of nanofluid and porous matrix along the diagonal, Figures 16(a)-(b) displays dimensionless temperature profiles for them as a function of ε at LTNE domain. From the graphs in Figures 16(a)-(b) one can notice that for all different values of the porosity, $\varepsilon =$ 0.4, 0.6, 0.8, 0.9 the dimensionless temperature profiles coincide with each other for both nanofluid and the solid matrix along the diagonal. These results indicate that the porosity ε does not have impact on the local thermal exchange between nanofluid and the porous matrix.

Da *θ along Y=2X-0.05*

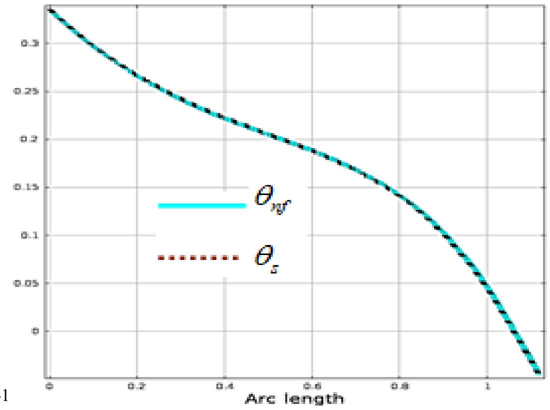

10^{-1}

(a)

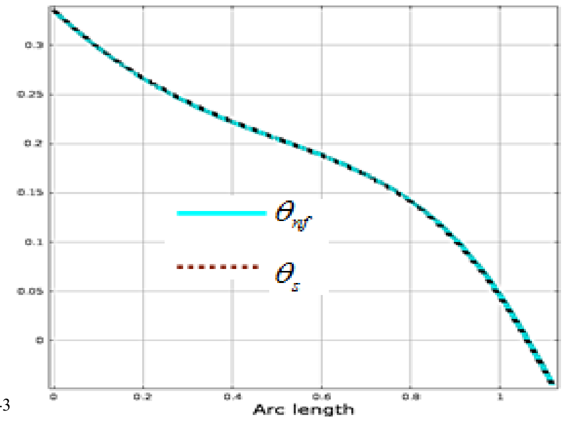

10^{-3}

(b)

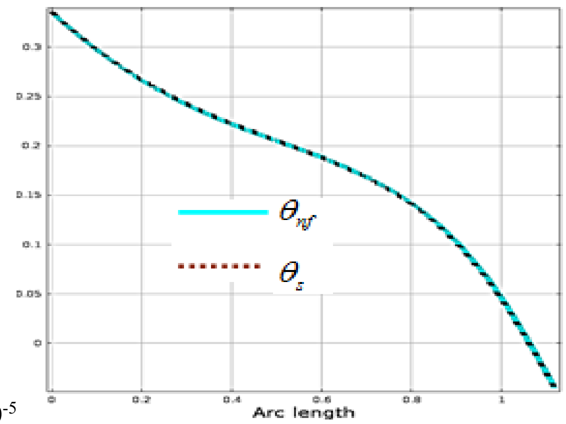

10^{-5}

(c)

Figures 12(a)-(c). Temperature distributions along the line $Y = X$ as a function of arc length varying φ when, τ=1 and Ni $= 10^5$, ε = 0.6, Da=0.1, Ø=0.05, Ra=10^5

Ø *θ along Y=X*

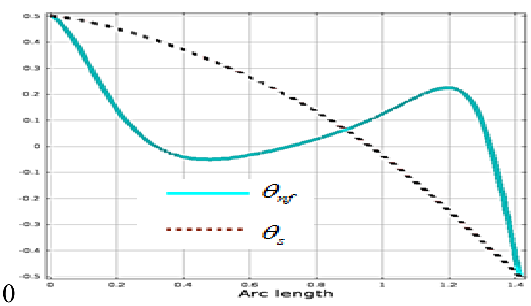

0

(a)

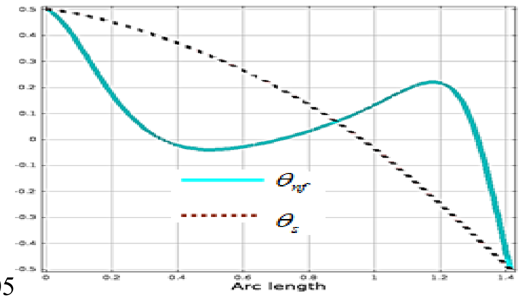

0.05

(b)

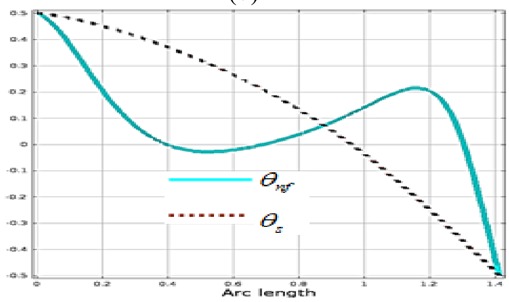

0.1

(c)

Figures 13(a)-(c). Temperature distributions along the line $Y = X$ as a function of arc length varying $\emptyset$ when, Da=0.1, Ra=10^5, τ=1, Ni=10, and ε=0.6

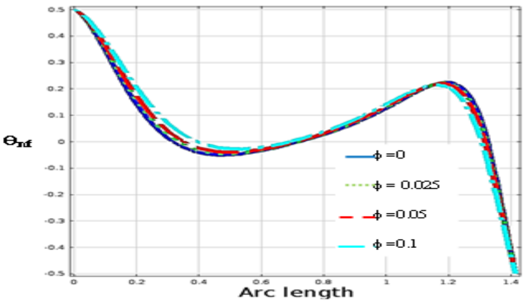

(a)

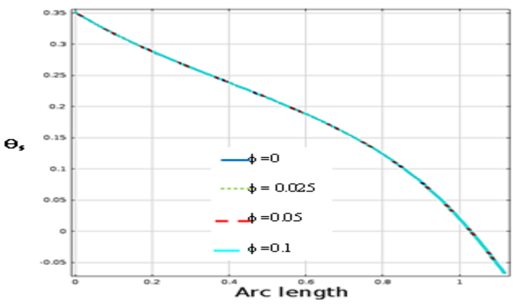

(b)

Figures 14(a)-(b). Temperature distributions (a) θ_{nf} and (b) θ_s along the line $Y = X$ for different values of $\emptyset$ at LTNE domain when, Ni=10, ε=0.6, Da=0.1, Ra=10^5 and τ=1

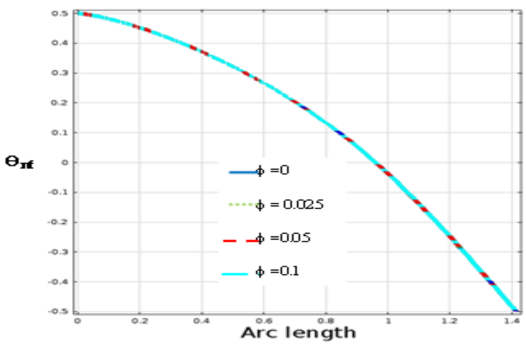

(a)

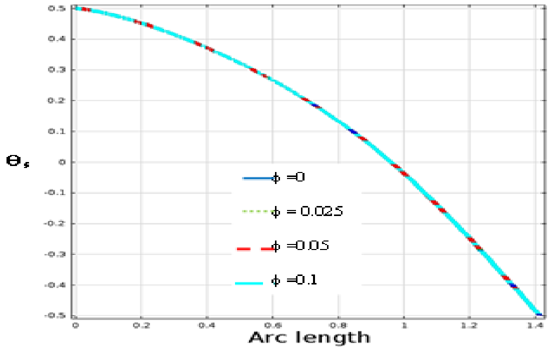

(b)

Figures 15(a)-(b). Temperature distributions (a) θ_{nf} and (b) $\theta_s$along the line $Y = X$ for different values of $\emptyset$ at LTNE domain when, Ni=10, ε=0.6, Da=10^{-5}, and Ra=10^5

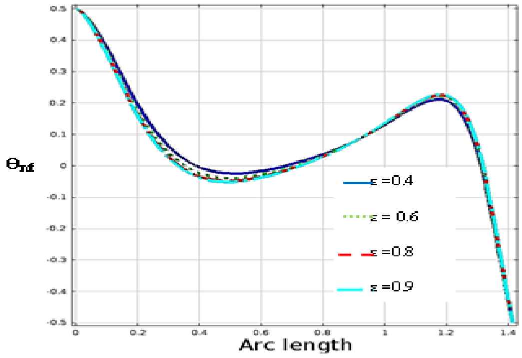

(a)

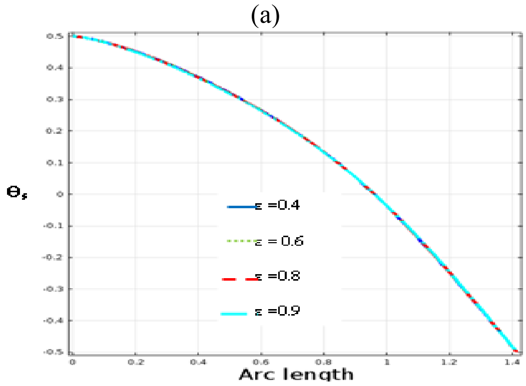

(b)

Figures 16(a)-(b). Temperature distributions (a) θ_{nf} and (b) $\theta_s$along the line $Y = X$ for different values of ε at LTNE domain when, Ni=10, ε=0.6, Da=0.1, Ra=10^5, and τ=1

5. CONCLUSIONS

In this study we investigated numerically the unsteady natural convective heat transfer in a nanofluid saturated porous right-angle trapezoidal cavity taking into consideration of LTNE state among the nanofluid and the porous matrix. On the other hand nanoparticles and the base fluid are considered to be in LTE state. Incompressible Cu-H_2O nanofluid is used as the passing fluid with homogeneous Aluminum foam having uniform pores as a porous medium. Two-temperature equations have been considered in this model, one for the nanofluid and another for the solid matrix. The heat transport configurations within the cavity are presented displaying isotherms. Moreover, LTNE model is used to describe the dimensionless temperature profiles within the cavity for nanofluid and porous matrix. The dimensionless temperature profiles were calculated along two different lines which are the diagonal ($Y = X$) of the cavity and along the line ($Y = 2X - 0.05$) which is close to the inclined wall of the enclosure.

From our studied numerical results, we conclude that exchange of heat among the nanofluid and the porous matrix is significantly controlled by the Nield and Darcy numbers. Thus, Darcy number is identified as an important parameter for regulating heat exchange between the nanofluid and solid matrix when passing nanofluid through a porous medium.

We found that for $\mathrm{Da} = O(10^{-5})$, the passing nanofluid and the solid matrix reach in thermal equilibrium regardless of the values of Nield number. Likewise, the nanofluid and the porous matrix reach in thermal equilibrium state when $Ni = O(10^{5})$ no matter what is the value of the Darcy number. The nanoparticles volume fraction and the porosity of the medium do not have much influence on the exchange of heat among the nanofluid and the porous matrix.

In addition, it is important and interesting to extend this study considering non-uniform pores of the porous medium taking into account porous matrix, base fluids, and solid nanoparticles are at LTNE states. A detailed research work in this line is in progress and the outcomes will be reported in a further communication.

ACKNOWLEDGEMENT

M. M. Rahman is grateful to the Sultan Qaboos University for funding under the grant IG/SCI/DOMS/18/10.

REFERENCES

[1] Choi SUS, Eastman JA. (1995). Enhancing Thermal Conductivity of Fluids with Nanoparticles. In: Siginer DA, Wang HP (Eds) Developments and Applications of Non-Newtonian Flows, ASME, New York.

[2] Wong KV, Leon OD. (2010). Applications of nanofluids: Current and future. Advances in Mechanical Engineeering. https://doi.org/10.1155/2010/519659

[3] Uddin MJ, Al Kalbani KS, Rahman MM, Alam MS, Al-Salti N, Eltayeb IA. (2016). Fundamentals of nanofluids: Evolution, applications and new theory. International Journal of Biomathematics and Systems Biology 2(1):1-32.

[4] Reddy MG. (2014). Influence of thermal radiation on natural convection boundary layer flow of a nanofluid past a vertical plate with uniform heat flux. International Journal of Heat and Technology 32: 1-7.

[5] Mahmoudi A, Mejri I, Abbassi MA, Omri A. (2014). Lattice Boltzmann simulation of magnetic field direction effect on natural convection of nanofluid-filled cavity. International Journal of Heat & Technology 32: 9-14.

[6] Mejri I, Mahmoudi A, Abbassi MA, Omri A. (2014). Magnetic field effect on natural convection in a nanofluid filled enclosure with non-uniform heating on both side walls. International Journal of Heat & Technology 32: 127-134.

[7] Bello SO, Olajuwon BI, Kuye SI. (2014). Convective heat and mass transfer in an mhd nanofluid in the presence of chemical reaction and thermal radiation. International Journal of Heat & Technology 32: 147-154.

[8] Rahman MM, Rosca AV, Pop I. (2015). Boundary layer flow of a nanofluid past a permeable exponentially shrinking surface with convective boundary condition using Buongiorno's model. International Journal of Numerical Methods for Heat & Fluid Flow 25(2): 299-319. https://doi.org/10.1108/HFF-12-2013-0361

[9] Rahman MM, Al-Rashdi MH, Pop I. (2016). Convective boundary layer flow and heat transfer in a nanofluid in the presence of second order slip, constant heat flux and zero nanoparticles flux. Nuclear Engineering and Design 297: 95-103. https://doi.org/10.1016/j.nucengdes.2015.11.021

[10] Uddin MJ, Alam MS, Rahman MM. (2017). Natural convective heat transfer flow of nanofluids inside a quarter-circular enclosure using nonhomogeneous dynamic model. Arabian Journal for Science and Engineering 42(5): 1883-1901. https://doi.org/10.1007/s13369-016-2330-0

[11] Uddin MJ, Alam MS, Al-Salti N, Rahman MM. (2016). Investigations of natural convection heat transfer in nanofluids filled horizontal semicircular-annulus using nonhomogeneous dynamic model. American Journal of Heat and Mass Transfer 3(6): 425-452. https://doi.org/10.7726/ajhmt.2016.1024

[12] Al-Weheibi SM, Rahman MM, Alam MS, Vajravelu K. (2017). Numerical simulation of natural convection heat transfer in a trapezoidal enclosure filled with nanoparticles. International Journal of Mechanical Sciences 131: 599-612. https://doi.org/10.1016/j.ijmecsci.2017.08.005

[13] Chandrasekar M, Kasiviswanathan MS. (2018). Variational approach to MHD stagnation flow of nanofluid towards permeable stretching sheet. International Journal of Heat and Technology 36(2): 411-421. http://dx.doi.org/10.18280/ijht.360205

[14] Bejan A, Kraus AD. (1987). Heat Transfer Handbook. New Jersey, Wiley, 1131-1180.

[15] Ingham DB, Pop I. (Eds). (2005).Transport Phenomena in Porous Media III 3, Oxford, Elsevier.

[16] Vafai K. (2005). Hand Book of Porous Media. 2nd edn New York, Taylor & Francis. https://doi.org/10.1201/9780415876384.

[17] Vafai K. (2010). Porous Media: Applications in Biological Systems and Biotechnology, Boca Raton, CRC Press.

[18] Vadasz P. (2008). Emerging Topics in Heat and Mass Transfer in Porous Media: From Bioengineering and Microelectronics to Nanotechnology 22, New York, Springer.

[19] Al-Amiri AM. (2002). Natural convection in porous enclosures: the application of the two-energy equation model. Numerical Heat Transfer: Part A: Applications 41(8): 817-834. https://doi.org/10.1080/10407780290059369

[20] Baytas AC, Pop I. (2002). Free convection in a square porous cavity using a thermal non-equilibrium model. International Journal of Thermal Sciences 41(9): 861-870. https://doi.org/10.1016/S1290-0729(02)01379-0

[21] Baytas AC. (2003). Thermal non-equilibrium natural convection in a square enclosure filled with a heat-generating solid phase, non-Darcy porous medium. International Journal of Energy Research 27(10):975-988. https://doi.org/10.1002/er.929

[22] Kasaeian A, Daneshazarian R, Mahian O, Kolsi L, Chamkha AJ, Wongwises S, Pop I. (2017). Nanofluid

flow and heat transfer in porous media: A review of the latest developments. International Journal of Heat and Mass Transfer 107: 778-791. https://doi.org/10.1016/j.ijheatmasstransfer.2016.11.074
[23] Beukema KJ, Bruin S, Schenk J. (1983). Three-dimensional natural convection in a confined porous medium with internal heat generation. International Journal of Heat and Mass Transfer 26(3): 451-458. https://doi.org/10.1016/0017-9310(83)90049-2
[24] Haajizadeh M, Ozguc AF, Tien CL. (1984). Natural convection in a vertical porous enclosure with internal heat generation. International Journal of Heat and Mass Transfer 27(10): 1893-1902. https://doi.org/10.1016/0017-9310(84)90171-6
[25] Kim GB, Hyun JM. (2004). Buoyant convection of a power-law fluid in an enclosure filled with heat-generating porous media. Numerical Heat Transfer, Part A: Applications 45(6): 569-582. https://doi.org/10.1080/10407780490277572
[26] Wu F, Wang G, Zhou W. (2014). Natural convection in a cavity filled with porous medium with partially thermal active sidewalls under local thermal nonequilibrium conditions. Journal of Porous Media 17(11): 983-997. https://doi.org/10.1615/JPorMedia. 17.i11.40
[27] Wu F, Wang G, Zhou W. (2015). A thermal nonequilibrium approach to natural convection in a square enclosure due to the partially cooled sidewalls of the enclosure. Numerical Heat Transfer, Part A: Applications 67(7): 771-790. https://doi.org/10.1080/10407782.2014.949189
[28] Rahman MM, Pop I, Saghir, MZ. (2019). Steady free convection flow within a titled nanofluid saturated porous cavity in the presence of a sloping magnetic field energized by an exothermic chemical reaction. International Journal of Heat and Mass Transfer 129: 198-211. https://doi.org/10.1016/j.ijheatmasstransfer.2018.09.105
[29] Nield DA, Bejan A. (2013). Convection in Porous Media. Springer Science & Business Media, 31-46. https://doi.org/10.1080/07373938908916581
[30] Nield DA. (2002). Modeling Fluid Flow in Saturated Porous Media and at Interfaces. Transport Phenomena in Porous Media II 1-19. https://doi.org/10.1016/B978-008043965-5/50002-7
[31] Baytas AC, Pop I. (2002). Free convection in a square porous cavity using a thermal nonequilibrium model. International Journal of Thermal Sciences 41(9): 861-870. https://doi.org/10.1016/S1290-0729(02)01379-0
[32] Hossain MA, Wilson M. (2002). Natural convection flow in a fluid-saturated porous medium enclosed by non-isothermal walls with heat generation. International Journal of Thermal Sciences 41(5): 447-454. https://doi.org/10.1016/S1290-0729(02)01337-6
[33] Wu F, Zhou W, Ma X. (2015). Natural convection in a porous rectangular enclosure with sinusoidal temperature distributions on both side walls using a thermal non-equilibrium model. International Journal of Heat and Mass Transfer 85: 756-771. https://doi.org/10.1016/j.ijheatmasstransfer.2015.02.039
[34] Pippal S, Bera P. (2013). A thermal non-equilibrium approach for 2D natural convection due to lateral heat flux: Square as well as slender enclosure. International Journal of Heat and Mass Transfer 56(1-2): 501-515. https://doi.org/10.1016/j.ijheatmasstransfer.2012.09.003
[35] Mahmoudi Y, Karimi N, Mazaheri K. (2014). Analytical investigation of heat transfer enhancement in a channel partially filled with a porous material under local thermal non-equilibrium condition: effects of different thermal boundary conditions at the porous-fluid interface. International Journal of Heat and Mass Transfer 70: 875-891. https://doi.org/10.1016/j.ijheatmasstransfer.2013.11.048
[36] Sheremet MA, Pop I, Nazar R. (2015). Natural convection in a square cavity filled with a porous medium saturated with a nanofluid using the thermal nonequilibrium model with a Tiwari and Das nanofluid model. International Journal of Mechanical Sciences 100: 312-321. https://doi.org/10.1016/j.ijmecsci.2015.07.007
[37] Tiwari RK, Das MK. (2007). Heat transfer augmentation in a two-sided lid-driven differentially heated square cavity utilizing nanofluids. International Journal of Heat and Mass Transfer 50(9-10): 2002-2018. https://doi.org/10.1016/j.ijheatmasstransfer.2006.09.034
[38] Sheikholeslami M, Shehzad SA. (2018). Simulation of water based nanofluid convective flow inside a porous enclosure via non-equilibrium model. International Journal of Heat and Mass Transfer 120: 1200-1212. https://doi.org/10.1016/j.ijheatmasstransfer.2017.12.132
[39] Mehryan SAM, Izadi M, Sheremet MA. (2018). Analysis of conjugate natural convection within a porous square enclosure occupied with micropolar nanofluid using local thermal non-equilibrium model. Journal of Molecular Liquids 250: 353-368. https://doi.org/10.1016/j.molliq.2017.11.177
[40] Brinkman HC. (1949). A calculation of the viscous force exerted by a flowing fluid on a dense swarm of particles. Flow, Turbulence and Combustion 1(1): 27. https://doi.org/10.1007/BF02120313
[41] Brinkman HC. (1949). On the permeability of media consisting of closely packed porous particles. Flow, Turbulence and Combustion 1(1): 81. https://doi.org/10.1007/BF02120318
[42] Ochoa-Tapia JA, Whitaker S. (1995). Momentum transfer at the boundary between a porous medium and a homogeneous fluid-II. Comparison with experiment. International Journal of Heat and Mass Transfer 38(14): 2647-2655. https://doi.org/10.1016/0017-9310(94)00347-X
[43] Brinkman HC. (1952). The viscosity of concentrated suspensions and solutions. The Journal of Chemical Physics 20(4): 571-571. https://doi.org/10.1063/1.1700493
[44] Maxwell JC. (1873). A Treatise on Electricity and Magnetism, Vol I, II, Oxford, Clarendon Press.
[45] Oztop HF, Abu-Nada E. (2008). Numerical study of natural convection in partially heated rectangular enclosures filled with nanofluids. International Journal of Heat and Fluid Flow 29(5): 1326-1336. https://doi.org/10.1016/j.ijheatfluidflow.2008.04.009
[46] Zienkiewicz OC, Taylor RL, Zienkiewicz OC, Taylor RL. (1977). The finite element method Vol 36. London, McGraw-Hill.
[47] Uddin MJ, Rahman MM. (2017). Numerical computation of natural convective heat transport within nanofluids filled semi-circular shaped enclosure using nonhomogeneous dynamic model. Thermal Science and Engineering Progress 1: 25-38. https://doi.org/10.1016/j.tsep.2017.02.001

[48] Al-Kalbani KS, Alam MS, Rahman MM. (2016). Finite element analysis of unsteady natural convective heat transfer and fluid flow of nanofluids inside a tilted square enclosure in the presence of oriented magnetic field. American Journal of Heat and Mass Transfer 3: 186–224. https://doi.org/10.7726/ajhmt.2016.1012

NOMENCLATURE

C_p	specific heat, J.kg.K^{-1}
Da	Darcy number
g	acceleration due to gravity, m.s^{-2}
h	interface heat transfer coefficient between the nanofluid and solid matrix
H	height of the enclosure
K	permeability
l	length of the top wall, m
L	length of the bottom wall, m
Ni	Nield number
Nu	Nusselt number
p	dimensional pressure, Pa
P	dimensionless pressure
Ra	Rayleigh number
t	dimensional time, s
T	Temperature, K
T_0	reference temperature
T_h	temperature of the hot wall, K
T_c	temperature of the cold wall, K
(u, v)	dimensional velocity components, m.s^{-1}
(U, V)	dimensionless velocity components
(x, y)	dimensional coordinates, m
(X, Y)	dimensionless coordinates

Greek symbols

α	thermal diffusivity, m.s^{-2}
β	coefficient of volume expansion, K^{-1}
τ	nondimensional time
ρ	fluid density, kg.m^{-3}
μ	dynamic viscosity, Pa.s
υ	kinematic coefficient of viscosity
θ	dimensionless temperature
ϕ	nanoparticles volume fraction
κ	thermal conductivity, W.m^{-1}.K^{-1}
λ	ratio of diffusivity
ε	porosity
δ	ratio of conductivity

Subscripts

nf	nanofluid
bf	base fluid
sp	solid particles
s	solid matrix